Valery G. Bondur, «Satellite Monitoring and Mathematical
Modelling of Deep Runoff Turbulent Jets in Coastal Water Areas»
in book Waste Water - Evaluation and Management, ISBN 978-953-307-233-3,
InTech, Croatia,2011,pp. 155-180

7

Satellite Monitoring and Mathematical Modelling of Deep Runoff Turbulent Jets in Coastal Water Areas

Valery G. Bondur
AEROCOSMOS Scientific Centre for Aerospace Monitoring, Russia

1. Introduction

One of the most important problems at the present time is the environmental pollution. Anthropogenic impacts on seas and oceans, and first of all on coastal water areas where more than half of the Earth population lives, makes the great contribution to this problem.
The most intensive effects on ecosystems of coastal waters have deep waste water outfalls (Israel, Tsiban, 1989). Intensive discharges of pollutants in the near-surface layer of the ocean lead to a progressive eutrophication and microbiological contamination of sea water and cause a disruption in the ecosystem's balance and drop in environmental bio-productivity. Therefore, it is important to organize monitoring of anthropogenic impacts on marine environment caused by deep runoffs.
Study and monitoring of such anthropogenic impacts is usually carried out using in-situ methods, which are of local character. Therefore, the use of aerospace methods and technologies to solve such issues is very promising (Bondur, 2004). This paper gives an overview of contemporary aerospace methods and means, as well as mathematical modelling of turbulent jets caused by deep runoffs, and possibilities of their application to monitor pollutions of coastal water areas. The focus is on the comprehensive studies which allow us to integrate remote and in-situ data with modelling results. For satellite monitoring, the methods are used based on the registration of deformations of surface wave spatial structure and hydrooptical inhomogeneities due to the interaction of deep runoff jets with the ocean surface and the near-surface layer.
Some results from the comprehensive monitoring of anthropogenic impacts on Mamala Bay water area (Oahu Island, Hawaii, USA) are also presented here, as well as data obtained for Black Sea water area near Gelenjik city which confirm these results.

2. Physical features of deep runoff turbulent jet propagation

The dumping of wastewater into the sea is usually from a continually operating source located in the bottom layer. Outfall devices can have various constructions, but all of them, as a result of their operation, create in the marine environment a turbulent jet or a series of jets, density of which differs from water density on the depth of source (Vladimirov et al., 1991). Because the water dumped into the sea is usually non-salty water containing different

impurities, its initial density, as a rule, is less than the density of the environment, therefore the jet floats. The main initial parameters of the turbulent jet are the flow rate Q (the amount of liquid moving through the cross-section of the jet in a unit of time), impulse or momentum (the product of the flow rate of a jet and its velocity) and the difference of water density $\Delta\rho$ in the jet (ρ) and in the sea (ρ_0) on the plane of the source, determining together with the flow rate a buoyancy of the jet (Ozmidov, 1986):

$$F = g\Delta\rho Q / \rho_0 , \tag{1}$$

where g is the gravity.

While the turbulent jet propagates, its flow rate increases because of its involvement into the movement of surrounding waters. If the medium is uniform in density and the difference between medium density and a jet density equals zero, when a jet propagates its impulse remains. Otherwise, only the horizontal component of impulse remains whereas the vertical component varies under the influence of buoyancy forces. If the medium is uniform in density, and its density is not equal to the density of the jet, then the jet floats (under the condition of linearity of the equation for state of water).

The main problem of water dumping into littoral water areas is the aim to "bury" jets in under layers, not allowing them to surface and pollute the upper layer. Therefore, outfall devices are installed, as a rule, in the regions with stable stratification (Vladimirov et al., 1991).

If we observe the fluid (Lagrangian) element of the floating jet in stably stratified medium then, because of intermixing with the surrounding waters its density increases, and the density of the surrounding water is reduced (element surfaces) and at the certain depth the difference in densities becomes zero - the jet will cease to surface (Bondur, Grebenyuk, 2001; Zhurbas, 1977).

To facilitate description of jet propagation processes, they are usually divided into 2 phases: active and passive (Bondur, Grebenyuk, 2001).

The active phase is a jet segment from the source up to the place where the level of turbulence (turbulent fluctuations of velocity) in the jet will cease to substantially differ from background, typical marine environment (without a jet). From the similarity principle and dimensions it is possible to establish that in stably stratified medium the duration of the active phase t_0 (time of transition of the fluid element of the jet from the source up to that place where the turbulence in the jet degenerates to levels comparable with the background) is defined as the characteristic time of free oscillations and conditionally can be estimated as a half of Brunt-Väisäla period:

$$t_0 = T / 2 = \pi \left[(g / \rho_0) \frac{\partial \rho}{\partial z} \right]^{-\frac{1}{2}} \tag{2}$$

At the end of the active phase, the surfacing of a jet ceases, and its further spreading happens approximately on one plane. Further, the jet makes only damped oscillations relative to that plane on which it was at the end of the active phase.

At the passive phase, the cross-section of a jet becomes significantly non axis-symmetric. Turbulent involvement ceases. Growth in vertical size practically does not happen and even can decrease because of the collapse phenomenon. The horizontal size grows, in

particular, due to collapse (Bondur, Grebenyuk, 2001; Ozmidov, 1986). As the jet continues to differ in temperature and salinity from surrounding water on the same plane, on the jet's side borders, Stern thermohaline instability may develop resulting in intrusion and stratification of the jet (Stern, 1960). Thus the jet forms a peculiar vertical "layered cake" and no longer exists as a whole. Intrusion stratification aides growth in the horizontal size of the area occupied by diluted wastewater. As the jet still has a thermohaline anomaly compensated in the density field, on its upper and lower boundaries, convective double diffusion processes like "salt fingers " (on that border where the temperature and salinity decrease with depth) and level-by-level convection (where the temperature and salinity grow with depth) may develop. (Ambartsumyan et al., 1995; Stern, 1960). Convective double diffusion processes can intensify vertical interchange more than on the order, promoting further dilution of dumped waters. Being passive, the jet is transferred by currents, the impurity disperses due to horizontal diffusion. The horizontal size of the area occupied the impurity increases as a result of the combined effects of the vertical shift (gradient) of the currents' velocity and vertical diffusion (so-called diffusion with shift of velocity). Separation of the suspended matter included in the jets occurs. Suspended matter, the density of which is less (more) than the density of water surface (sink) relative to the position of the sewage jet and can reach the surface (or bottom) of the sea. Knowing the hydraulic fineness of the suspended matter, distance from the plane of a surfacing of the jet to the surface (or bottom) of the sea, rate of dilution at the end of the active phase and the effective coefficient of the horizontal diffusion, it is possible to estimate the time of arrival of the suspended matter at the surface (or bottom), the area of contamination and the concentration of the pollutants. The process of separation is not significant in the active phase, because of its short duration (the first tens minutes) (Ozmidov, 1986).

At deep wastewater outfalls lower than the level of the thermocline, there is turbulization of the lower boundary of the density shift, formation of vortex structures of various scales, generation of internal waves, and related fields of currents, shaping of convective motions stipulated by desalting of the under layer of the medium (salt fingers), and appearing of pollutants which cause changes in waver characteristics and affect the water area ecosystem (Bondur, 2004; Bondur, Grebenyuk, 2001; Bondur et al., 2009a).

3. Applicability of space methods for monitoring anthropogenic impacts on coastal water areas

Significant success has been achieved recently in the area of development and application of aerospace methods and technologies for ocean remote sensing. Their main advantages are: wide coverage; real time monitoring; capability to work in any areas of seas or oceans difficult to access; capability to acquire data with various spatial and temporal resolutions and over wide areas of the electromagnetic wave spectrum; measurement of a wide spectrum of parameters; high accuracy of obtained data, especially when combined with in situ measurements; capability to network aerospace information, as well as retransmit data received from monitoring by airplane, helicopter, ships and buoy stations to customers (Bondur, 2004).

Turbulent jets of deep runoffs cause changes in various parameters of the marine environment which can be remotely sensed using aerospace means (Bondur, 2004; Bondur, Grebenyuk, 2001). Deep plume propagation cause deformation of the surface due at direct

interaction with surfacing jets, and also generation of surface waves by vortex structures. Besides this, there is a distortion of the space-time structure of the disturbance by internal waves, turbulence and layers of surfactants (Bondur, 2004; Bondur, Grebenyuk, 2001). For registration of such distortions, optical and radar equipment installed on aerospace platforms can be used (Bondur, 2004).

Under the influence of deep plumes, there is also a change hydrooptical characteristic of the seawater, which is exhibited in increased turbidity and changed colour due to the increase of scattering and light absorption owing to a raise in concentration of suspended and dissolved organic matter. To detect such phenomena, it is possible to use passive (spectral, multispectral, and hyperspectral monitoring), as well as active (lidar) optical methods (Bondur, 2004; Bondur, Zubkov, 2005; Bondur et al., 2006a).

Deep plumes cause water surface temperature variations in current fields, upwelling areas, turbulence, and internal waves, etc. For registering changes in temperature, infrared and passive microwave sensing methods (Bondur, 2004; Bondur, Grebenyuk, 2001) can be used.

In the field of the deep plumes there is a change in the physical and chemical characteristics of the marine environment, which is exhibited in magnification of the content of dissolved organic matter, phosphorus, nitrogen, heavy metals, dissolved oxygen, and also in a change of temperature and salinity of seawater. These effects also can be identified using various remote methods. For example, the content of dissolved organic matter can be measured using lidars by analysing spectra of combinational scattering and fluorescence, excited by laser radiation. For measuring the remaining physical and chemical parameters of the environment, the laser-spark method, a method for laser correlation spectroscopy etc. can be used (Bondur, 2004, Bondur, Zubkov, 2001).

Due to the long-term existence of various processes related with deep runoffs, a rise in phytoplankton concentration is possible, resulting in a change in spectral characteristics of the fluorescent signals which also can be remotely registered (Bondur, 2004).

This paper focuses on studying spatial distribution of low-contrast small-scale structures related to deep runoffs. These structures manifest themselves in the changes of surface waves and in heterogeneities of ocean surface layer hydrodynamical and hydrooptical parameters. For this study we use the methods of spatial spectral analysis and the methods of processing high resolution multispectral satellite imagery, as well as the integration of satellite imagery processing results with hydrophysical data obtained during sea truth measurements, as well as with mathematical modelling results.

4. Methodological features of comprehensive satellite and in-situ monitoring of deep runoff impacts on coastal water areas

Comprehensive monitoring of anthropogenic impacts on coastal water areas was performed under the international project. The main goal of this project was detection of negative impact of deep wastewater runoffs on the Mamala Bay water area and Oahu Island resorts ecosystems (Honolulu, Hawaii, USA) (Bondur, 2006; Bondur & Filatov, 2003; Keeler et al., 2003; Gibson et al., 2006; Bondur et al., 2007; Bondur & Tsidilina, 2006).

The main source of anthropogenic load was the discharge of treated wastewaters through the Sand Island outfall device. Its diffuser is 1036 m long and has 282 ports. It is located on

70 m depth and at a distance of 3.8 km from the shore. The average flow rate is 4.48 m^3/s (Fischer et al., 1979).

Fig. 1 presents the scheme of comprehensive monitoring which illustrates the peculiarities of its techniques. In this figure we can see the location of the Sand Island Outfall, images of main satellites, ships, some sensors and remote platforms used for the monitoring (Bondur, 2006).

Periodical space imaging of the bay water area was performed during the monitoring using:

- Optical high resolution sensor of IKONOS and QuickBird satellites providing imagery of 0.61 – 1.0 m resolution and multispectral imagery of 2.44-4.0 m resolution;
- Radar sensor of RADARSAT (8 and 25 m resolution, λ=5.6 cm wavelength, HH polarization) and ENVISAT (~ 25 m resolution, λ=5.6 cm, HH, VV, VH polarization);
- Hyperion hyperspectral sensor (~ 30 m resolution, 220 spectral bands in the range of 0.4-2.5 μm), as well as ALI sensor (~ 10 m resolution (panchromatic mode) and ~ 30 m (multispectral mode), 10 spectral bands in the range of 0.4-2.4 μm of EO-1 satellite;
- ASTER sensor (15 m resolution in visible and near-IR band, 30 m in mid-IR and 90 m in far-IR band), TERRA satellite;
- Multispectral MODIS sensor (250 m resolution in visible and near-IR band, 500 m in mid-IR and 1 km in far-IR band), TERRA and AQUA satellites;
- Multispectral sensors of International Space Station were used (~ 2 m resolution (panchromatic mode) and ~ 5 m (multispectral mode);
- Data acquired by "Meteor-3M", NOAA, and GOES weather satellites were involved.

To verify remote sensing data obtained with space assets, the following sea truth data were used: wind conditions; parameters of surface waves (wave buoys); current fields (ADP sensors and drifters); temperature fields (thermistor strings); temperature and salinity profiles (TS, CTD, and XBT sensors); microstructure data (MSS, TOMI), hydrooptical (AC-9, Secchi disks) and hydrobiological (Niskin bottles) parameters; and tidal mode (Bondur, 2006; Bondur et al., 2007.

Fig 1 shows the locations of stations for measurements of temperature vertical profile time dependences (thermistors), as well as parameters of current velocity fields (ADP). Navigation paths for CTD measurements, determination of hydro-optical (AC-9 sensor and Secchi disks) and hydro-biological parameters, as well as wave buoy paths for surface wave spectra measuring are given in Fig. 1. Dashed line denotes the bay area where vertical and horizontal measurements using dropped and towed microstructure sonde were carried out (Bondur, 2006; Bondur et al., 2007).

Descriptions of sensors used for sea truth measurements are given in (Bondur et al., 2007; Bondur & Filatov, 2003; Gibson et al., 2006; Keeler et al., 2004; Wolk et al., 2004).

A large number of satellite images from various satellites were obtained during experiments carried out in the Mamala Bay water area. The total data volume exceeded 150 Gb (Bondur, Tsidilina, 2006).

Original satellite images and sea truth data, as well as complementary information (digital maps, meteorological and GPS data, etc.) were recorded to the archive. Then, data pre-processing was carried out to enhance image quality. After pre-processing, the data was subjected to further thematic processing and comprehensive analysis (Bondur & Tsidilina, 2006).

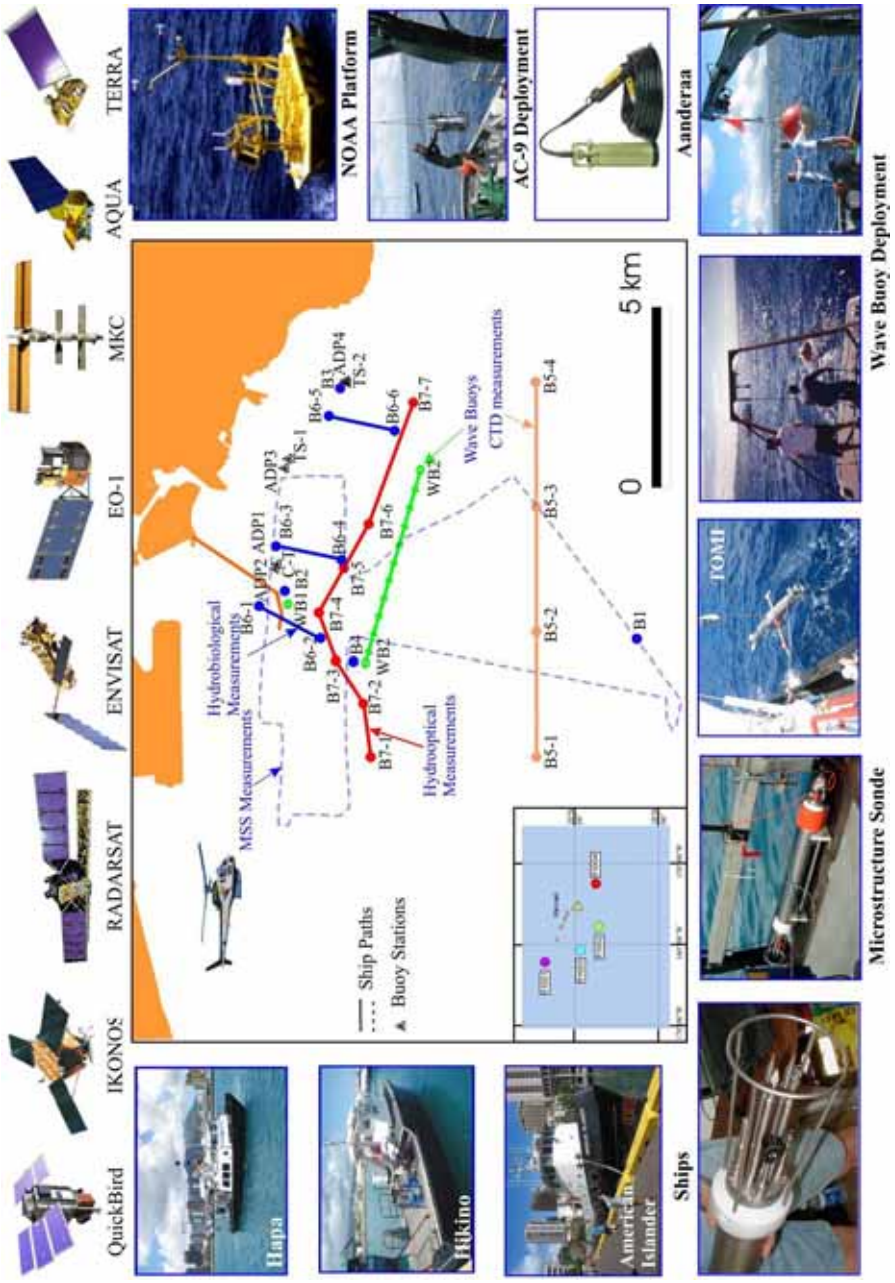

Fig. 1. Schematic for comprehensive monitoring of the coastal water area near Oahu Island (Hawaii)

5. Comprehensive monitoring results

5.1 Detection of "quasi-monochromatic" structures in the areas of deep outfalls using satellite imagery

Among the most important monitoring results was the detection in high resolution satellite imagery of "quasi-monochromatic" structures in the area where disturbances caused by deep plumes interacted with surface waves.

The processing of high resolution satellite images was carried out using a technique based on the method of remote spatial-frequency spectrometry (Bondur, 2004). The original satellite images were divided into fragments of 1024x1024 and 2048x2048 pixels, ensuring sampling volumes sufficient to attain required statistical precision for spatial spectra evaluation and achieve the spatial resolution needed to estimate geometrical characteristics of surface anomalies caused by deep outfalls. These fragments were used to evaluate 2D-spatial spectra and their cross-sections in different directions; to determine informative indicators of these spectra; to compute parameters of spectral harmonics; to carry out statistical analysis of informative indicators; to detect abnormal areas related to the deep outfall and to evaluate dimensions of these anomalous areas. The technique described above was used for the processing of IKONOS and QuickBird imagery obtained for the days of comprehensive experiments in the Mamala Bay water area (Hawaii, USA) and in Gelenjik Bay (Russia).

Fig. 2 shows an example of the processing of the IKONOS satellite image taken on September 2, 2002. The satellite image fragment in Fig. 2,a shows three areas highlighted to the south from the outfall diffuser (orange colour) in the area of estimated plume manifestation (anomaly) and one area far from the diffuser (background). Fig. 2,b shows 2D spatial spectrum of the background fragment, and Fig. 2,c shows three spectra of anomalous fragments in the outfall area (conditional colours). As can be seen in Fig. 2a,c, the spectra of the anomalous fragments clearly show additional narrow "quasi-coherent" spectral components (spatial frequency $\nu \sim 0.01075$ m^{-1}, average spatial period for these components is $\bar{\Lambda} = 93$ m, and average widening is $\Delta\bar{\Lambda} \sim 4$ m). Thus, the condition

$$\Delta\Lambda << \Lambda , \tag{3}$$

is fulfilled, therefore such additional wave components can be called "quasi-monochromatic".

Their generation is related with surface manifestations of disturbances caused by turbulent jets of deep outfall. There are no such spectral harmonics in the background spectrum (Fig. 2,b).

Fig. 2,d,e shows one dimensional frequency spectra obtained using wave buoys at the moment of space imaging (11 hours, 20 minutes, local time) in the outfall area (e) and in the background area (d). As can be seen from the one-dimension spectrum in Fig. 2,e an additional "quasi-coherent" spectral component corresponds to spatial frequency ν=0.01075 m^{-1} (wavelength $\Lambda \sim 93$ m), what conforms to the spatial periods of "quasi-monochromatic" components detected by 2D spectra of the space image fragment showing the anomaly.

Fig. 2,f shows the result from identification of a surface anomaly caused by the deep outfall. This anomaly was estimated taking into account changes in spatial spectra of high resolution satellite imagery caused by additional "quasi-coherent" spectral harmonics.

In this figure, anomalous fragments of the image (1x1 km^2 size) which correspond to two dimensional spectra displaying "quasi-monochromatic" wave components are filled with

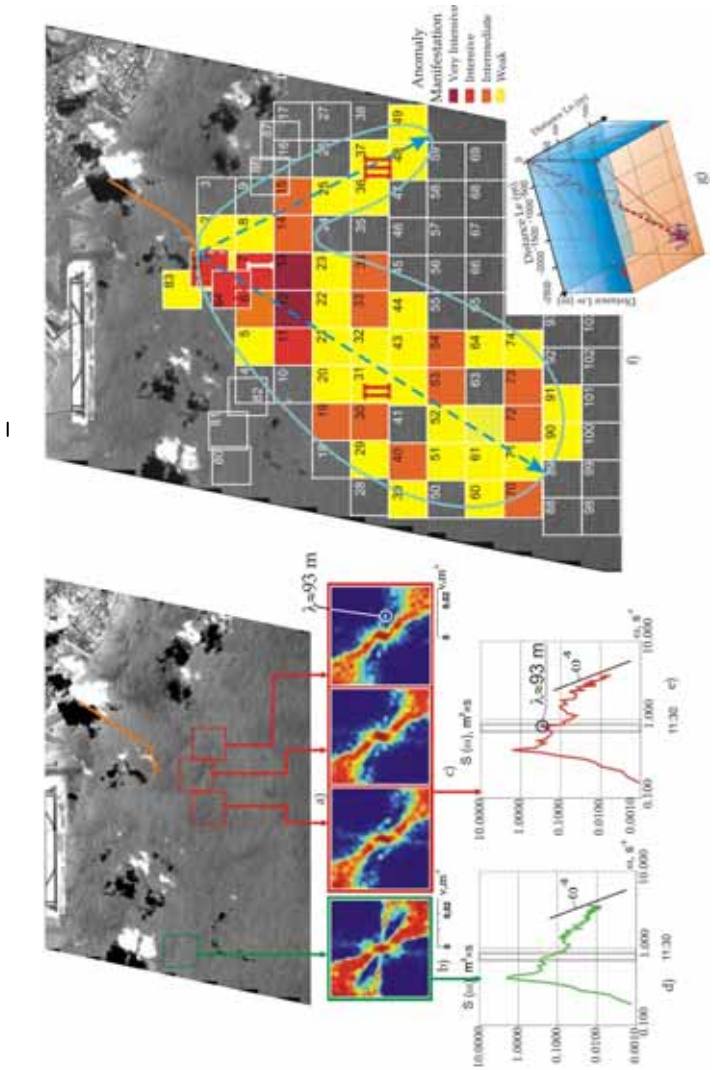

Fig. 2. Revealing surface anomaly using satellite image (IKONOS, ~ 1 m resolution, 2 Sept. 2002). This anomaly is caused by deep outfall impact on surface waves, and is detected by the generation of "quasi-monochromatic" components. a - fragment of the initial image with 4 pieces for processing (in the deep outfall area (anomaly) and background); b - 2D background spectrum; c - 2D spectra of anomalous fragments with "quasi-coherent" spectral harmonics with Λ=93 m wavelength; d – one-dimensional frequency spectra obtained by wave buoys in the background area; e - one-dimensional frequency spectra of deep outfall area (with "quasi-coherent" spectral harmonic corresponding to 93 m wavelength); f - satellite image with detected during the processing anomalous areas of various intensity (very intensive, intensive, medium, weak) related with "quasi-monochromatic" wave component s; g - progressive-vector diagram for current velocity field

different colours. The colours correspond to various anomaly intensities, depending on the intensity (energy) of additional harmonics. The entire zone of anomalies zone (outlined in blue) has the two-lobe "mitten-like" shape, the larger lobe of which (length more than 11 km and width of about 6 km) is elongated in the south west direction (angle about 215°) and the second, smaller lobe (length about 6-7 km, width about 2 km) is stretched in the south east direction (with angle about 154°).

Fig. 2,g presents a progressive-vector diagram based on current velocity data for the experimental area (Bondur & Filatov, 2003). The analysis of Figs. 2,g and 2,f shows that the dominant direction of the elongation of the surface anomaly with "quasi-monochromatic" wave components almost coincide with dominant current direction at the moment of the satellite imaging.

Some example results of surface anomaly detection are given in Figs. 3 and 4. These anomalies are related with deep outfalls and appear as additional "quasi-monochromatic" wave components.

Fig. 3 shows the results of spatial spectral processing of the QuickBird space image obtained on September 14, 2003.

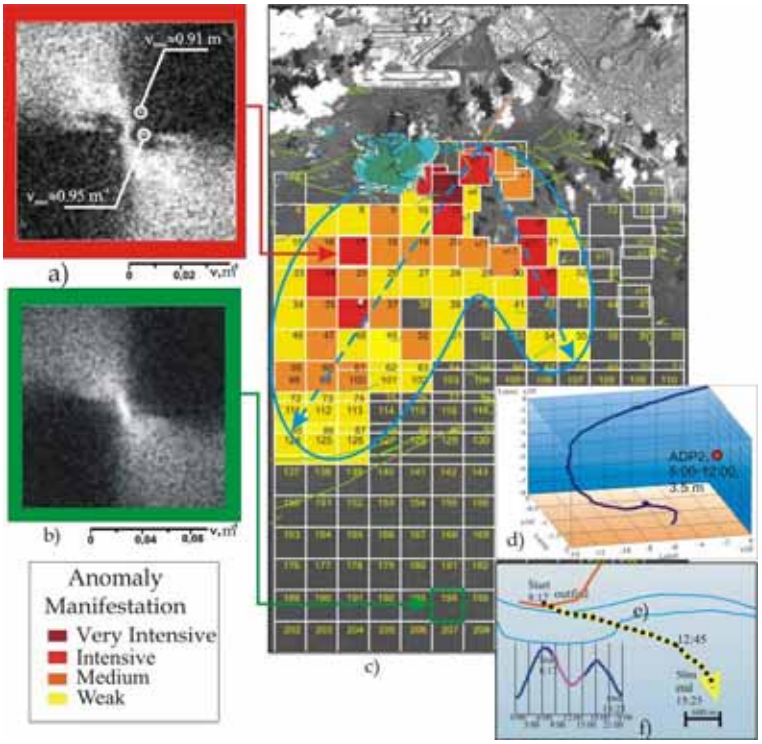

Fig. 3. QuickBird image processing results (September 14, 2003). a) – 2D spatial spectrum with two pairs of "quasi-coherent" spectral maxima in the anomalous area; b) – Background spectrum; c) – The anomaly due to "quasi-monochromatic" wave components in the area of deep outfall; d) – Current field progressive-vector diagram (ADP measurements from 5:00 till 12:00 LT at a depth of 3.5 m); e) – Drifter moving trajectory; f) – Tide diagram

As for the experiment whose results are shown in Fig. 2, on the September 14, 2003 near the diffuser, additional "quasi-coherent" spectral harmonics were detected (Fig. 3,a) and were not detected (Fig. 3,b) far from the diffuser (background). However, as opposed to the case from Fig. 2, in this experiments there were detected two pairs of additional narrow spectral harmonics (see Fig. 3,a)with wavelengths Λ_1 = 91 m and Λ_2 = 95 m matching the condition (3). And the pairs of these "quasi-coherent" spectral harmonics were oriented in different directions, what indicates generation of two systems of "quasi-monochromatic" wave components on the sea surface propagating in different directions (Fig. 3,a).

Even more complicated wave pattern was detected during the processing of images taken on other days. E.g., a great number of pairs of narrow spectral maxima differently oriented were revealed in this QuickBird image (September 3, 2004) fragments (1.33 × 1.33 km^2) (see Fig. 4,b). These maxima matched the condition (3) what indicated the presence of a multimode system of "quasi-monochromatic" wave components on the sea surface (see Fig. 4). Average wavelengths were 43 to 117 m (see Fig. 4,b). There are no such "quasi-coherent" harmonics in background spectra (Fig. 4,c).

Unfortunately, the lower right part of satellite imaging area was covered with clouds, what did not allow us to study the anomalies in this area in more details.

Shapes of surface anomalies detected in the deep outfall area on September 14, 2003 (See Figs. 3,c) and September 3, 2004 (See Fig. 4,a) taking into account spectral harmonics are similar (mitten-like shape), though have some differences (size, direction, intensity, inner structure).

The processing results for satellite images obtained on different days of experiments indicate the repetition of observed surface interests related with deep outfall impacts on Mamala Bay water area. A similar stable form may result from the regular south-western transfer of water mass in the surface layer (~220^o - 235^o) detected in data collected using the ADP (Acoustic Doppler Profiler) (Bondur & Filatov, 2003; Bondur et al., 2007). This can be seen in Fig. 3,d which presents a 3D progressive vector diagram built based on data collected by the ADP2 station (the closest to the diffuser) at a depth of 3.5 m on September 14, 2003. The analysis of current fields enables us to conclude that the south-western direction of water mass transfer prevailed at all depths for a long time (currents velocity was in the range of 10-20 cm/s). However, this direction has changed to the southeast near the time of space imaging (September 14, 2003, 11:16 LT). This is related with the change in tidal phase (see Fig. 3,f). This resulted in the appearance of two lobes in the surface anomaly detected by space imagery. South-eastern propagation of wastewaters was also revealed in current measurements carried out using a Lagrange drifter near the diffuser (see Fig. 3,e) (at a depth of about 50 m, velocity 13 cm/s) (Bondur et al., 2007).

These results are similar to those obtained on other days of experiments.

Summarising all obtained data for Mamala Bay, let's indicate that average wavelengths of "quasi-monochromatic" waves varied between $\overline{\Lambda}$ = 30…200 m over different points of surface anomaly and different days. And directions of anomalous spectral harmonics varied between 45° and 180°.

The shape of surface anomaly is usually two-lobe (mitten-like) with max size of 11 to 25 km.

5.2 Physical mechanisms causing "quasi-monochromatic" wave components in deep outfall areas

Appearance of surface wave anomalies related to discharges of non-salty water into salty marine environment is caused by a series of hydrophysical mechanisms (turbulence,

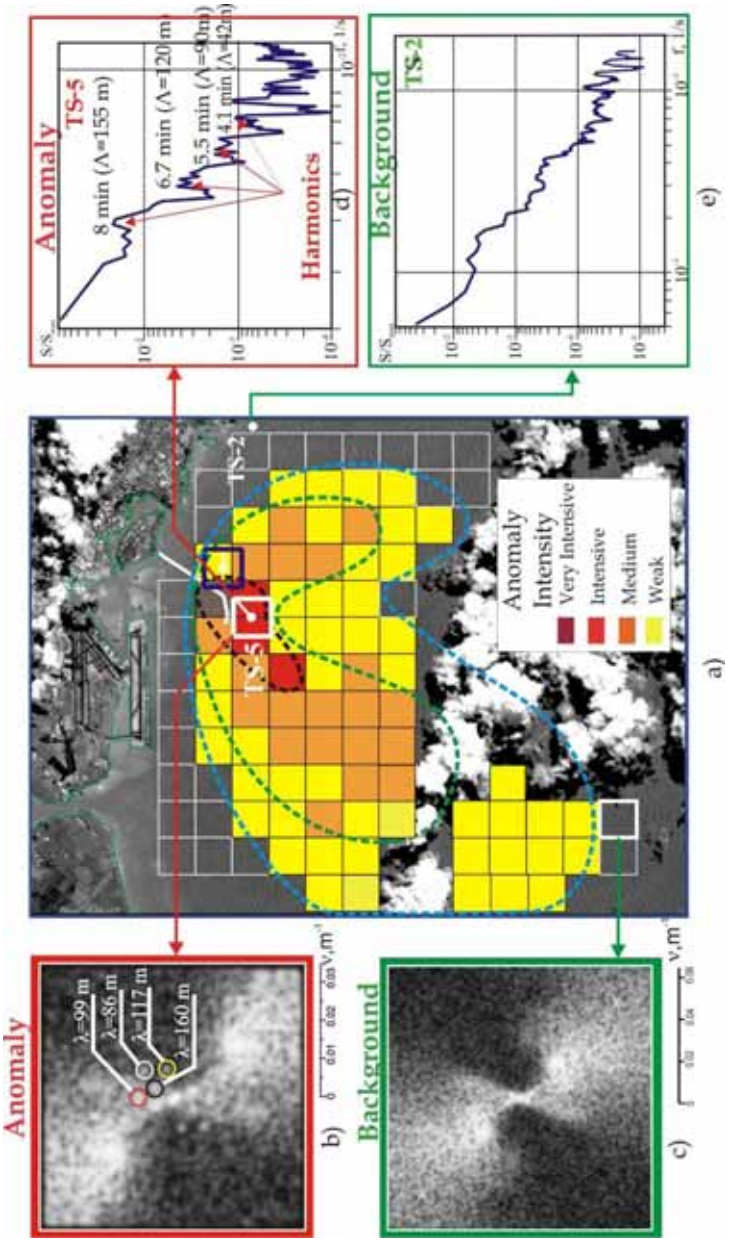

Fig. 4. Detection of "quasi-monochromatic" wave components in satellite image (QuickBird, September 3, 2004) spectra: original image showing deep outfall manifestation area - (a); spectrum with multimode "quasi-coherent" harmonic system - (b); background spectrum - (c); internal wave spectra near the diffuser (TS-5) - (d); and outside the anomaly (TS-2) with indicated periods and appropriate lengths of internal waves - (e)

buoyant vortexes, internal waves, oil and surfactant films, and etc.), most important of them is an interaction of short-period internal waves and surface waves (Bondur, 2004; Bondur, Grebenyuk, 2001). To confirm this, let's analyze spectral parameters of internal waves near and at the distance from the diffuser. The results of measurement of temperature profiles (every 30 s) using moored Thermistor Strings are used for this purpose. These results are to be compared with characteristics of "quasi-monochromatic" wave components on the sea surface detected taking into account spatial spectra of satellite image in the area of deep outfall.

The comparison will be made for the case of experiments in Mamala Bay on September 3, 2004. The results of fragment-by-fragment (1.33x1.33 km²) spatial spectral analysis of QuickBird satellite image taken on that day are shown in Fig. 4,a. As we see in Fig. 4,b, multimode structure of narrow "quasi-coherent" spectral harmonics are clearly seen in the anomalous spectrum. These harmonics are absent in the spectrum for background (Fig. 4,c). These spectral harmonics correspond to the surface wave systems with average lengths $\overline{\Lambda}$ = 43; 86; 99; and 117 m. Average width of these harmonics is $\overline{\Lambda}$ ~ 5 – 7 m. Thus, the condition $\overline{\Delta\Lambda} << \overline{\Lambda}$ is fulfilled that allow us to term these detected components "quasi-monochromatic".

Study of high-frequency internal waves will be carried out using analysis of 27.5°C isotherm depth spectra for 2 hour time period (10:00 – 12:00 LT). (Bondur & Filatov, 2003; Bondur et al., 2007).

Fig. 4,d presents an internal wave spectrum created using data obtained at TS-5 located 600 m to the south from the outfall diffuser (see Fig. 4,a). A similar spectrum for TS-2 far from the diffuser near Waikiki Beach (see Fig. 1) is given in Fig. 4,e). Unlike in the background spectrum (TS-2), ultrahigh frequency spectral components (with 4.1 – 8 min periods) caused by internal waves generated by deep outfall are clearly seen in the spectrum of T=27.5°C isotherm depth near the diffuser.

Lengths of such ultra short internal waves estimated based on measurement results for their periods using the dispersion relation for such waves and measured in the experiment Brunt-Väisälä frequencies $N=(gd\rho/\rho dz)^{1/2}$, where ρ is the density; z is the depth.

The internal wave period is $T_{IW} = 2\pi/\varpi_{IW}$.

The internal wave frequency is derived from the dispersion relation:

$$w_{IW} = gk_{IW}\frac{\Delta\rho}{\rho}\left[cth(kh) + cth(k_{IW}H)\right]^{-1} \quad (4)$$

where:

$k_{IW} = 2\pi/\Lambda_{IW}$ - is the wave number for internal waves;

Λ_{IW} is the internal wave length;

$\Delta\rho = \rho_2 - \rho_1$ is the difference between lower and upper layer density.

The phase velocity of internal waves is the following:

$$C_{IW} = \frac{w_{IW}}{k_{IW}} \pm \left\{ g\frac{\Delta\rho}{\rho} / k_{IW}\left[cth(k_{IW}h) + cth(k_{IW}H)\right] \right\}^{1/2} \quad (5)$$

In our case we deal with ultrashort internal waves matching the following condition:

$$k_{IW}h >> 1 \text{ and } k_{IW}H >> 1 \quad (6)$$

Taking into account (5) and (6), the phase velocity is the following:

$$C_{IW} = \left(\frac{\rho \Delta \rho}{\rho} \right) / 2k_{IW} \tag{7}$$

The internal wave length is:

$$\Lambda_{\mathrm{IW}} = T_{\mathrm{IW}} \cdot C_{\mathrm{IW}} \tag{8}$$

Using these equations and taking into account the measurement results, wavelengths for our case are Λ = 42; 90; 120 and 155 m for appropriate spectral maxima (see Fig. 4,d). Similar harmonics are absent in the internal wave background spectrum (see Fig. 4,e), what is the evidence of their direct relation with such a determined source as a permanent deep outfall. The comparison of lengths of ultrashort internal waves (TS-5 Station) with "quasi-monochromatic" harmonic lengths of 2D spatial spectrum for the satellite image fragment covering the area around this station confirms their very good correlation (1 – 5 % difference). This is the evidence of the validity of "internal wave" hypothesis of generation of multimode system of "quasi-monochromatic" surface structure caused by a deep outfall. Physical mechanisms of internal wave interaction with surface waves were analysed in (Bondur, 2004; Bondur, Grebenyuk, 2001).

5.3 Radar satellite imagery analysis

Radar imaging using the RADARSAT and ENVISAT satellites was carried out during the monitoring of anthropogenic influence caused by the deep outfall in the Mamala Bay water area. Radar image pre-processing consists of calibration (σ^0 (sigma nought) calculation), speckle-noise elimination, geo-coding and formation of improved images by applying equalization procedures. Thematic processing included the following main stages: scanning of pre-processed imagery by a statistically significant sliding window, and calculation of informative attributes in each window, as well as statistical analysis, choice of optimal informative attributes and automated classification (Bondur, 2004; Bondur, Starchenkov, 2001). To verify the results of radar image processing, data on wind fields obtained by ships and ground stations, as well as hydrophysical data were used. Use of additional information allowed us to decrease error probability during classification of radar imagery down to 0.04-0.06 using the Neyman-Pearson criterion.

Detection of areas related to the deep outfall and anomalies caused by the dynamic influence of wind was carried out using automated classification procedures based on various types of informative attributes (Bondur, 2004; Bondur, Starchenkov, 2001). Physical mechanisms of ocean surface radar image formation were described in (Bondur, 2004), as well as registered parameters were analyzed. The presence of disturbed ocean surface revealing in the variations of Bragg component of reflected radio waves (Bondur, 2004) made possible the detection of the deep outfall in Mamala Bay water area against the anomalies caused by wind flows from Nuuanu Valley and Manoa Valley.

The results of anomaly detection induced by Sand Island Outfall are given in Fig. 5. In this Figure different colours designate various radar signal intensities. Such surface anomalies are caused by deformations of high frequency (5 – 10 cm wavelengths) surface waves under the influence of deep outfalls which can be registered by a radar (due to Bragg mechanism) (Bondur, 2004).

Maximal dimensions of the surface anomaly caused by wastewater discharge from Sand Island are: max length is 24 km, max width is 7.6 km. The direction of elongation is ~250°, what matches the dominant current directions at the moment of radar imaging.
Max length of the anomaly due to Honouliuli outfall is ~5 km, and max width is ~2.3 km.
More details of the results of radar imagery obtained during monitoring can be found in (Bondur, 2004; 2005; Bondur, Starchenkov, 2005).

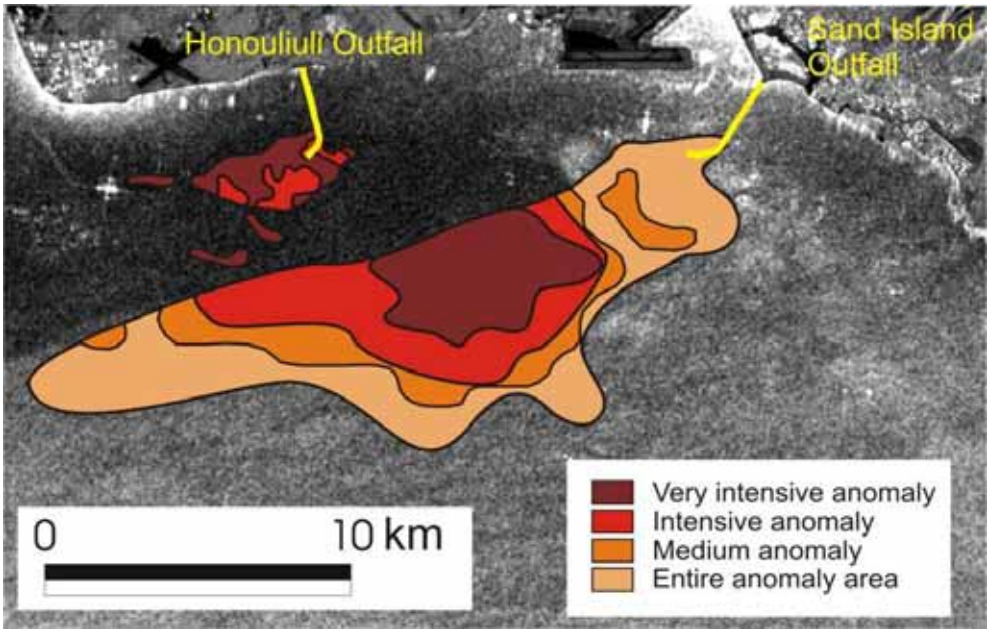

Fig. 5. Detecting the anomaly caused by the Sand Island and Honouliuli outfalls using the RADARSAT image of August 12, 2004

5.4 Summarizing surface effects of anomalies caused by deep outfall and detected using satellite imagery

Contours of anomaly propagation areas caused by a deep outfall and detected by spatial spectral processing of optical satellite imagery (a) and radar satellite imagery (b) are summarized in Fig. 6. These results were obtained for various days of comprehensive monitoring under various meteorological conditions (tide-and-ebb phases, current and wind directions and velocities, surface waves, thermocline location, etc.). The analysis of Fig. 4 shows that despite having significant difference (in dimensions, shape, propagation area) in the studied anthropogenic influence manifestations they have definite common features for each of data class obtained using various sensors. These features are appearing in rather local nature of similar anomaly manifestations, and relative shape stability for each type of sensors. The exclusion is the anomaly detected from RADARSAT image (September 11, 2003) under conditions of calm (wind speed was 1-1.5 m/s) (Bondur, 2004; 2005).
Differences in anomaly manifestations detected from optical and radar imagery denote various significant environment parameters registered by these sensor types.

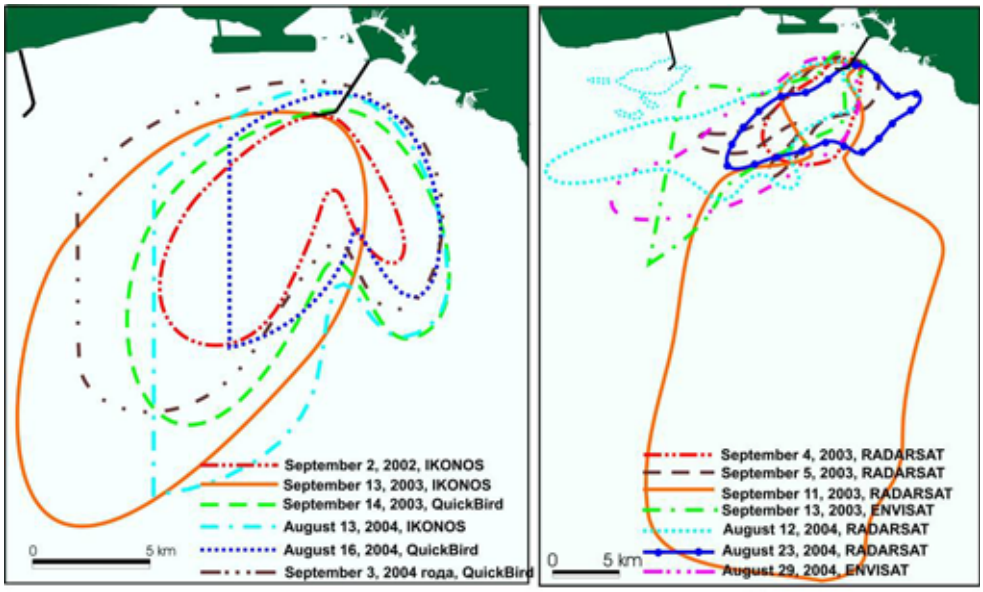

Fig. 6. Propagation areas for anomalies caused by the deep outfall in Mamala Bay (Hawaii)detected in optical (a) and radar (b) satellite images for different days under various hydrometeorological conditions

5.5 Anomalies of hydrooptical characteristics detected using high resolution satellite imagery and sea truth data

The processing of high resolution (2…4 m) multispectral images was carried out using the characteristics of relative signal variety in red (R), green (G), and blue (B) spectral bands of 60 – 80 nm width. The processing technique used the following basic procedures (Bondur, 2004; Bondur, Zubkov, 2005): synthesizing the colour image from separate bands (RGB-synthesis); interpreting imagery to mark out clouds, ships and their traces, land, and unclouded marine surface; selecting fragments of the full scene of an image for the area of interest for further processing; filtering; decorrelation stretch to remove correlation of spectral bands; parametric and non-parametric classification; combination of classes; colour coding.

To correct brightness image distortions caused non-uniform sensitivity of the CCD camera, additional procedures consisting in removing brightness transversal trend within each fragment; and brightness band interleveling based on statistic parameter use.

To verify the results of multispectral satellite imagery processing in the studied area, sea truth measurements were carried out using AC-9 hydrooptical equipment and various hydrophysical equipment at the moments of time close to satellite imaging time (Gibson et al., 2006; Bondur et al., 2006a; 2007)/ The gauge was deployed from the *Klaus Wyrtki* ship down to a depth of 150 m. Values of absorption factor and attenuation were measured using AC-9 equipment at nine wavelengths (in 412 to 715 nm spectral band) at each station (B6) located in the area of the outfall. Vertical profiles of these values were created for each station (Bondur et al., 2006a). To process AC-9 data we used the method based on the Haltrin-Kopelevich linear bio optical model (Kopelevich, 1983; Haltrin & Kattawar, 1993).

Fig. 7 presents the examples of multispectral QuickBird image processing (September 14, 2003; 11:16 LT imaging time). In this Fig. we can see: image fragment (16.5 x 16.5 km^2) synthesized from RGB bands of the original image (a); interim processing result consisting in obtaining pixel-by-pixel band signal ratios blue/green, in a convolution with mask and classification with further smoothing (b); result of combination of classes of similar brightness with colour palette changing (c); re-combination of classes, detection and outlining of anomalies (d).

The analysis of processing result shows that in the area of the Sand Island outfall diffuser (right part of Fig. 7,d) anomaly of subsurface ocean layer hydro-optical characteristics is evident.

Maximal size of this anomaly is about 6 km. Inside of this area more contrast extensive anomaly (~ 3.5 km length) oriented in south direction, is detected. Another distinct surface anomaly caused by oil spill due to leakage from a tanker during pumping to onshore reservoirs is evident. Rather small anomaly of hydro-optical characteristics caused by another outfall (Honouliuli) in Mamala Bay is seen on the left (see Fig. 7,d). Effectiveness of the applied processing technology is confirmed by the fact that on original images anomalies caused by the outfall are not seen.

Similar results were obtained after processing other multispectral satellite imagery as well as multispectral data (Bondur, 2004; Bondur, Zubkov, 2005; Bondur et al., 2006a).

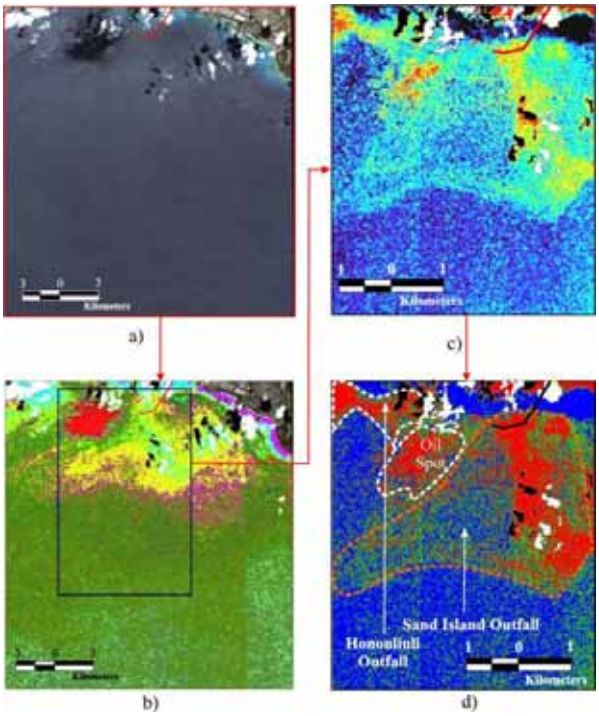

Fig. 7. Example of QuickBird multispectral image processing. a) original synthesized images; b) processed fragment; c) classification with smoothing by a window; d) combination of classes; e) final result

For the comparison with satellite imagery processing results, absorption and attenuation factors were used which had been obtained from AC-9 data at the wavelength of λ=0.488 μm, where sunlight absorption near the Hawaii was close to the minimum (Erlov, 1980). Also, AC-9 spectral band coincided with the centre of QuickBird blue band.

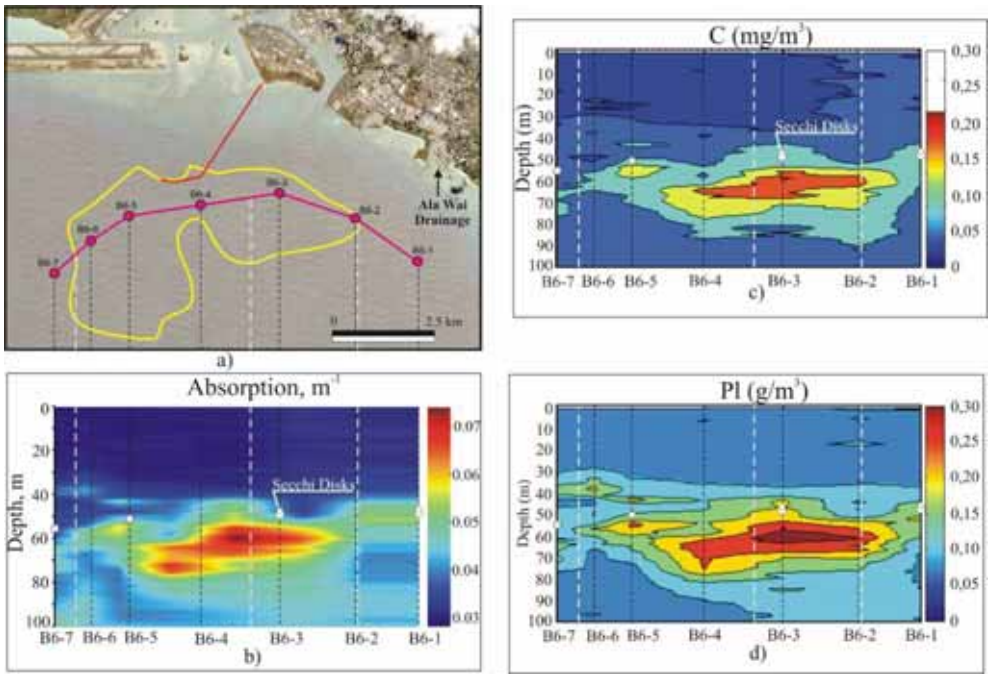

Fig. 8. Comparison of the anomaly detected using QuickBird multispectral imagery (September 3, 2004) (a) with 2D cross-sections of absorption at 0.488 μm wavelength (b); chlorophyll C (c) and large particles (d) concentrations based on AC-9 data. ○ – Secchi disk max visibility (b-d)

Fig. 8.a presents the outlined area of hydrooptical parameter anomaly detected using the multispectral QuickBird image of September 3, 2004 near the deep outfall and ship trajectory with indicated points where hydrooptical measurements had been carried out. Fig. 8 shows 2D distributions of absorption at λ = 0.488 μm (b), as well as chlorophyll C (c) and large particle (d) concentrations based on AC-9 data.

The results obtained by Secchi disks have shown than at B6-3 and B6-5 Stations (near the diffuser) maximum visibility was 48-51 m, while at B6-7 Station (far from the diffuser) it was 55.5 m. It is evident, that at B6-3 and B6-5 Station visibility decreased because of high concentrations of various substances (organic, suspended particles, end etc.) contained in wastewaters.

The processing analysis have shown the high level of coincidence both of western and eastern anomaly boundaries detected using the satellite multispectral images with the anomaly detected using hydrooptical data. The divergence of the results is 100 – 200 m.

Similar results were obtained during multispectral and hyperspectral satellite data (HYPERION). Max anomaly size was 5 – 20 km (Bondur, 2004); Bondur & Zubkov, 2005; Bondur et al., 2006a).

Thus, the comprehensive analysis of the collected data have allowed us to interpret unambiguously the processing results for multispectral imagery obtained during the monitoring of anthropogenic impacts on the water environment.

6. Modelling the propagation of turbulent deep plumes

6.1 The model employed

A mathematical model described in (Bondur, Grebenyuk, 2001; Bondur et al., 2006b; 2009b) has been used to study the propagation features of turbulent jets of contaminated waters discharged into Mamala Bay. The jet propagation is described with a system of seven ordinary differential nonlinear equations that characterize the balance of the horizontal and vertical components of the momentum, the heat consumption, the salinity, and the jet coordinates with the system being supplemented with the equation of the state of the sea water. These equations have been obtained by integrating the equations of the motion, continuity, and heat and salt balance under the assumption of scaling of the distributions of the velocity, temperature and salinity in the cross section of the jet (Bondur et al., 2006b).

When deriving the equations, we considered a turbulent jet that was injected at the depth z into the aquatic medium at angle of Θ_0 to the sea line in the xz plain. The medium was assumed to be incompressible and quiescent, and its density $\rho_a(z)$ was depth dependent with $d\rho_a/dz < 0$, which means the stable stratification of the medium (Bondur et al., 2006b).

The equation system looked as follows (Bondur et al., 2006b; 2009b):

$$\frac{d}{ds}(ub^2) = 2\alpha ub\,, \tag{9}$$

$$\frac{d}{ds}(u^2b^2\cos\Theta) = 0\,, \tag{10}$$

$$\frac{d}{ds}(u^2b^2\sin\Theta) = 2g\lambda^2b^2\frac{\rho_a-\rho_0}{\rho_0}\,, \tag{11}$$

$$\frac{d}{ds}[ub^2(T_a-T)] = \frac{1+\lambda^2}{\lambda^2}b^2u\frac{dT_a}{ds}\,, \tag{12}$$

$$\frac{d}{ds}[ub^2(S_a-S)] = \frac{1+\lambda^2}{\lambda^2}b^2u\frac{dS_a}{ds}\,, \tag{13}$$

$$\frac{dx}{ds} = \cos\Theta\,,\ \frac{dz}{ds} = \sin\Theta \tag{14}$$

$$\rho = \rho(T,S) \tag{15}$$

where $T_a(s)$ and $S_a(s)$ are the temperature and salinity of the medium, $T(s)$ and $S(s)$ are the temperature and salinity of the jet; $\alpha = 0.057$ is the entrainment coefficient; $b = b(s)$ is the characteristic half-width of the jet, and $1 = 1.16$ is a constant; s is the coordinate along the jet axis, r is the radial coordinate, $u(s)$ and $\rho(s)$ are the jet's axial velocity and density, $\rho_0 = \rho_a(0)$ is the reference density.

This system can be supplemented by an equation for the mean time t of the propagation of a fluid element along the trajectory of the jet:

$$dt = \frac{ds}{\overline{u}} = \frac{2ds}{u}, \tag{16}$$

where the mean velocity is determined from the condition that the Gaussian distribution of the velocity is substituted with a constant velocity $\overline{u}$ = u/2 in the section of the jet with a radius $\overline{b} = \sqrt{2b}$ at constant discharge and momentum.
The use of this model (9) – (16) makes possible the calculation of the resulting depth and the thickness of the jet propagation layer (the Ozmidov scale (Ozmidov, 1986)) in the stratified medium, dilution, and other parameters. A detailed description of the model is given in (Bondur et al., 2006b; 2009b).

6.2 Modelling results

When performing the model calculations, the following specifications of the Sand Island facility were used: the mean total discharge rate was Q = 4.64 m^3/s, the mean rate of the discharge from a single diffuser orifice was Q_0 = 0.0163 m^3/s, the velocity of the jet exiting the diffuser orifices was U_0 = 3 m/s, the depth level of the diffuser site was H = 70 m, and the temperature of the discharged waters was T_C = 25-27.5°C (Fischer, 1979). It was supposed that non-salty water discharge took place.
The data of the hydrophysical measurements (Bondur et al., 2007; Bondur & Tsidilina, 2006; Gibson et al., 2006; Wolk et al., 2004) were used to understand the stratification of the aquatic medium. It is worth noting that there are strong tidal currents that substantially influence the diverse hydrophysical processes, including the propagation of the turbulent jets of the discharged waste water (Bondur et al., 2008, Bondur et al., 2006a; Bondur & Filatov, 2005; Merrifield & Alford, 2004).
The hourly mean vertical density profiles plotted for eight time moments during the period from 13:00 September 1 to 13:00 September 2, 2002, are shown in Fig. 9,a. During this period of research, the intense density jump layer was located at depths of 30-50 m. The trajectories of propagation of floating-up jets in the mentioned time periods are shown in Fig. 9,b.
The graphs of the level of the floating-up jet and the density gradients for eight time moments during the period from September 1 to September 2, 2002, are shown in Fig. 10,a.
It is seen from these figures that, in the period considered, the jet did not rise higher than 36 m, i.e., not higher than the location of the density jump. The density jump with a strong gradient prevented the floating up of the jet closer to the surface.
Using the model developed, we also obtained estimates of the initial dilution of the sewage water. The graphs of the variation of the dilution Q/Q_0 and the density gradient $\Delta\rho/\Delta z$ for the period of research are shown in Fig. 10,b. It is seen from this figure that the weakest stratification of the seawater corresponds to the maximal value of the dilution of the discharged waters.
The outcomes of the model calculations of the initial dilution and the jet floating-up depth at thermistor chain locations from August 14 until August 26, 2004 are shown in Figs. 11,a,b. Under the stratification conditions characteristic of the site of station Ta, the jet remained mainly submerged (Fig. 11,b), excluding the shorter time periods when the diffuser occurred at the base of an internal tidal wave of large amplitude, when the jet floated up for a short time. The enlarged fragments of Fig. 11,b are shown in Figs. 11,c and 11,d. They represent the short-period jet surfacing: (c) from 15:14 on Aug. 15 to 13:50 on Aug. 16; (d) from 23:50 on Aug. 20 to 21:02 on Aug. 21.

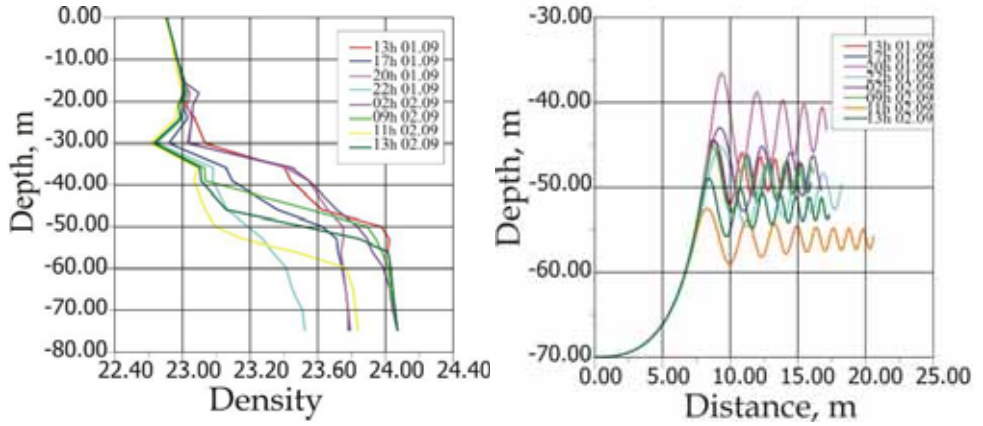

a) b)

Fig. 9. Vertical profiles of the seawater density in Mamala Bay during the period from 13:00 on September 1 to 13:00 on September 2, 2002 (a); and trajectories of propagation of turbulent floating-up jets of deep outfalls calculated from the data of the density profiles (b).

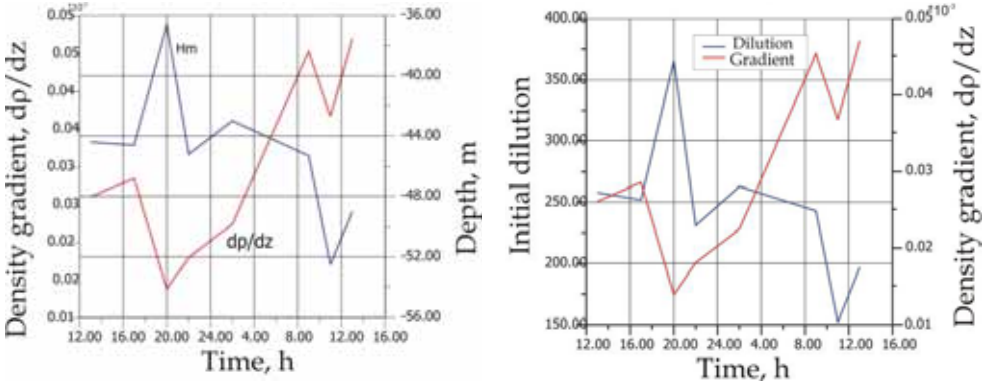

a) b)

Fig. 10. Comparison of the parameters of jet propagation with the characteristics of the medium stratification (September 1 – 2, 2002): (a) time evolution of the level of float up of the jet *Hm* and the density gradient $d\rho/dz$; (b) time evolution of the initial dilution of the sewage waters and the density gradient $d\rho/dz$

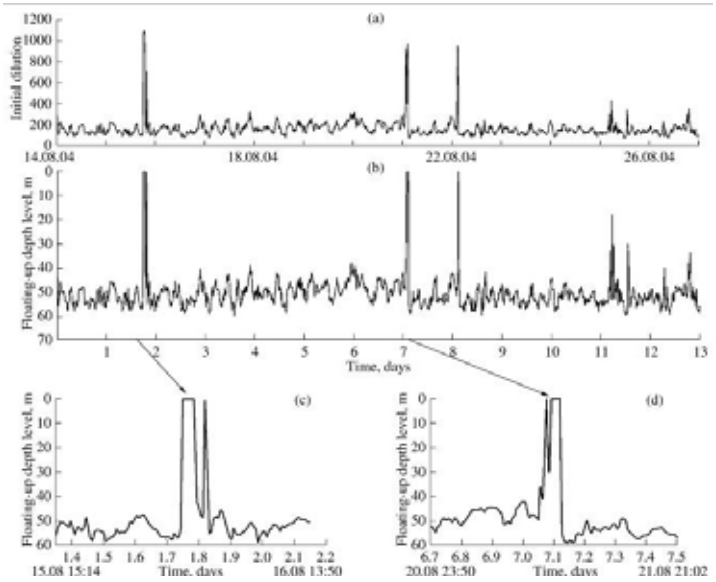

Fig. 11. Model calculations of the initial dilution (a) and the floating-up depth of the jet (b) from Aug. 14 to 26, 2004; enlarged fragments of Fig. 10,b for two short jet surfacing events from Aug. 15 (15:14) to 16 (13:50) (c) and from Aug. 20 (23:50) to 21 (21:02) (d)

6.3 Comparison of modelling and experimental data

A comparison of the parameters of the deep-water outfall discharges obtained on the basis of the experimental measurements with the results of the model calculations allows us to test whether the mathematical model applied is adequate and check the accuracy and reliability of the model estimates obtained.

Profiles of the spatiotemporal distributions of the (a) turbidity, (b) salinity, and (c), temperature of the seawater plotted on the basis of the microstructure measurements near the diffuser on September 2, 2002, from 12:15 to 15:20 are shown in this Fig. 12.

It is clearly seen from these profiles that, during the period analyzed, the discharge waters ascended to a depth of 45 m.

The levels to which the jet of sewage waters floated up calculated using the model in the period from 9:00 to 18:00 on September 2, 2002, are shown in Fig. 13,a. It is seen from the figure that, during the period from 12:00 to 16:00, the model estimate of the mean level of the floating up is equal to ~44 m, which is in good agreement with the data of the experimental measurements (~45 m). During the experiments from a research vessel on September 6, 2002 at 14:48, an anomalous spot at the sea surface was found near the diffuser. A photo of this surface anomaly taken by Professor C. Gibson is shown in Fig. 13,b.

Figure 13,c shows the outcomes of the model calculations for the same day and time period from 07:30 to 11:45. The model indicated the surfacing of the jet from 07:50 to 08:15, which is in perfect agreement with the occurrence time of the anomaly. A surface anomaly related to the floating up of the discharged waters was observed near the diffuser in 2004. A still picture of the anomaly taken on August 12, 2004 at 08:00 is given in Fig. 13,d. Similar events took place during the experiments of 2002 (Bondur et al., 2006b).

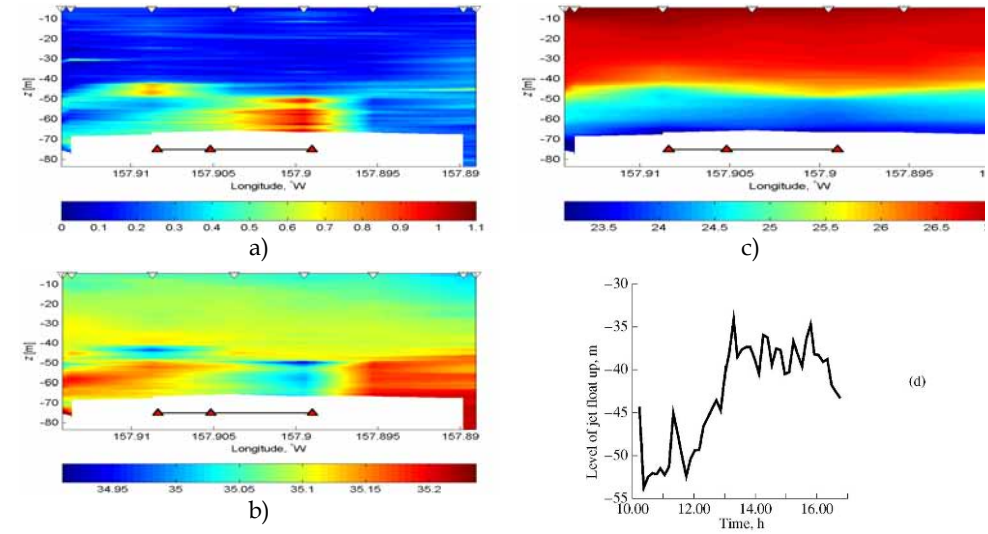

Fig. 12. Comparison of the model estimates of the parameters of the jet with the data of experimental measurements: vertical profiles of the (a) turbidity, (b) salinity, and (c) temperature on the basis of the measurements with an MSS profiler on September 2, 2002 during the period from 14:15 to 15:20; and (d) model estimates of the depth of the sewage water jet float up in the period from 9:00 to 17:00 on September 2, 2002.

Jet floating-up was also registered by AC-9 hydrooptical sensor (see Fig. 13,f). Fig. 13,e shows an example of 2D distribution of large particle concentration obtained by AC-9 (see subsection 4.4). The analysis of Fig. 13,e have shown that the increased concentration of large particles related with the deep outfall for B6-1 – B6-7 measuring track (see Fig. 8,a) was detected at 40-70 m depths, and the jet appeared on the surface at B6-2 and B6-6 points, and max concentration near the surface in the diffuser area (B6-4 and B6-5 points).

The good correspondence of the model's estimates of the propagation characteristics of the discharged water jets with the spatial patterns of the results of the hydrophysical and hydrooptical measurements corroborates the idea of the adequacy of the description of the turbulent jet propagation mechanism in the coastal aquatic areas based on our mathematical model.

7. Conclusion

The analysis of physical features of deep plume propagation in coastal water areas has been carried out, as well as capabilities to detect the impact of these plumes on marine environment have been grounded.

Based on high resolution (0.6 – 1.0 m) satellite image processing results, it has been established that in 2D spectra of their fragments "quasi-coherent" spectral harmonics are observed. These harmonics correspond to "quasi-monochromatic" (multimode sometimes) wave systems on the sea surface, having Λ = 30-200 lengths, and $\Delta\Lambda$ ~ 3-5 m widening, which also can be registered by wave buoys. The analysis of physical mechanisms causing these harmonics, performed by spectra of isotherm depths, have shown that these effects are

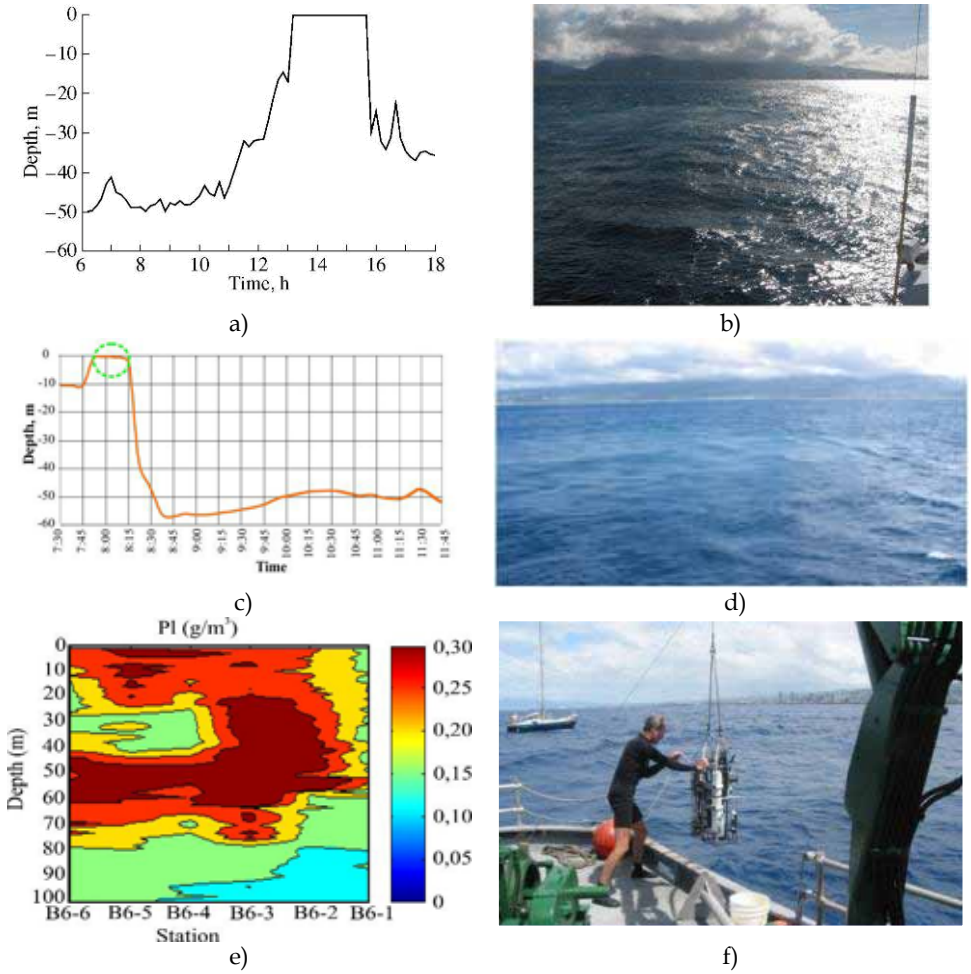

Fig. 13. Comparison of the model estimates of the parameters of the jet with the data of experimental measurements: (a) and (c) Model estimates of the float-up depth of the sewage jet in the period from 6:00 to 18:00 on September 6, 2002 (a) and from 07:30 to 11:45 on August 12, 2004 (c); (b) and (d) Photos of the surface anomaly caused by the deep-water discharge measured from a ship near the diffuser on September 6, 2002, at 14:48 by K.Gibson (b) and at 08:00 on August 12, 2004 (d); 2D profile of large particle concentration obtained by AC-9 (e); AC-9 deployment (f)

due to ultrashort internal waves generated by turbulent deep plumes in the stratified medium.

It has been established that surface anomalies which are characterized by the presence of "quasi-monochromatic" surface wave systems detected in the areas of deep outfall usually have two-lobe mitten-like shape. Its shape is quite stable, and dimensions varied between 11-23 km. Their intensity depends on outfall device operation mode, as well as by instability of hydrodynamical and meteorological modes of the studied water areas and tide influence.

As a result of high resolution (1-4 m) multispectral satellite image processing, there have been detected small-scale hydrooptical anomalies caused by intensive deep outfalls, and theirs geometry has been determined (5-20 km max). The comprehensive analysis of satellite image processing results and sea truth data has shown that the dimensions and propagation directions of these anomalies almost coincide with spatial distributions of hydrooptical parameter fields. This indicates the adequacy and efficiency of this method to study deep wastewater outfall impact on coastal water areas.

The processing of radar satellite imagery was carried out using specially developed methods providing online computer-aided detection and classification of surface anomalies. The comprehensive analysis of this processing results together with sea truth data have allowed us to detect the anomalies of high frequency surface waves (comparable with radar wavelength) in the areas of deep outfalls, to determine their variability depending on meteorological and hydrodynamical modes in the water area.

The model developed was used to estimate the parameters of a floating-up jet of deep wastewater discharge from Sand Island into the basin of Mamala Bay (Hawaii) depending on the season and discharge operation mode. The estimates of the float-up depths of the jet and the initial dilution of the jet were estimated on the basis of model calculations using experimental data on the vertical profiles of the water temperature and salinity under the actual conditions of stratification in the study region at various times. It is shown that the further propagation of the wastewater jet (first of all, at the depth of floating-up) depends on tidal events and internal waves generated by tides. The model estimates of the parameters of the wastewater discharge were compared with the results of experimental measurements. Good agreement was found, which indicates that the physical mechanisms of the propagation of turbulent jets in a stratified medium are adequately described by the model.

The results from the Mamala Bay monitoring (Hawaii, USA) are also confirmed by the data obtained in the Black Sea water areas near Gelenjik city (Russia).

Taking into account the big volumes of wastewater discharged into the water area of Mamala Bay (~ 70 mln. gallons/day), the presence of significant quantity of polluting substances (despite of good treatment system) and high requirements to seawater conditions in recreational zone of Honolulu city, some measures aimed to decrease anthropogenic load on the ecosystem of Mamala Bay are proposed based on the results of satellite monitoring.

1. In case of unfavorable conditions (tides, onshore current and wind directions (to Waikiki Beach), absence of thermocline), it is expedient to reduce the discharge rate as much as possible by accumulating wastewater in special WWTP reservoirs.

Under favorable conditions (ebbs, southern and southwestern directions of currents, south and southwest winds, expressed thermocline) it could be advised to increase the discharge rates since this is the best circumstances for their disposal.

2. To provide reliable information on favorable and unfavorable conditions and on water area environmental situation, it is necessary to maintain permanent monitoring of major parameters in Mamala Bay water area (current fields, CTD-measurements, wind speed and direction, air temperature, etc.), as well as to perform permanent aerospace monitoring by means of processing and analysis of remotely sensed data comparing it with the results of in-situ measurements.
3. Increase the density of wastewaters for their better disposal, e.g. by adding salt or diluting with seawater. Decrease volume of discharged waters in the coast part by

closing a part of diffuser ports at its north side. Increase the level of wastewater treatment by applying new technologies.

Such nature-preserving measures can be undertaken also for other water areas under intensive anthropogenic influence.

The presented results confirm the efficiency of aerospace methods and technologies, as well as methods of mathematical modeling deep turbulent plume propagation to monitor anthropogenic impacts on coastal water areas.

8. References

Ambartsumjan E.N., Astavin V.S., Bojarintsev V.I. etc. Estimation of the possibility of the exit of hydrodynamic perturbations onto the surface of ocean at the outflow of sewage from immersed dumps.-M: Institute of Applied Mathematics Russian Academy of Science " hydro physics ", 1995, p. 33.

Bondur V.G. Aerospace methods in Modern Oceanology. In: "New Ideas in Oceanology". Vol. 1: Physics. Chemistry. Biology. // Ed. by M.E. Vinogradov, S.S. Lappo, - M.: Nauka, 2004, p.p. 55 – 117 (In Russian).

Bondur V.G. Complex Satellite Monitoring of Coastal Water Areas 31st International Symposium on Remote Sensing of Environment. ISRSE, 2006, 7 p.

Bondur V.G., Filatov N. Study of physical processes in coastal zone for detecting anthropogenic impact by means of remote sensing. Proceeding of the 7 Workshop on Physical processes in natural waters, 2-5 July 2003, Petrozavodsk, Russia. p.p. 98-103.

Bondur V.G., Filatov N.N., Grebenuk Yu.V., Dolotov Yu.S., Zdorovennov R.E., Petrov M.P., Tsidilina M.N. Studies of hydrophysical processes during monitoring of the anthropogenic impact on coastal basins using the example of Mamala Bay of Oahu Island in Hawaii. // Oceanology, Vol. 47, No 6, pp. 769-787.

Bondur V.G., Grebenyuk Yu. Remote indication of anthropogenic influences on marine environment caused by deep outfalls, Issledovanie Zemli is kosmosa, 2001, №6, p.p. 49-67 (In Russian).

Bondur V.G., Grebenyuk Yu.V., Sabinin K.D. Peculiar Discontinuities in Small-Scale Currents at the Shelf in the Area of Natural Convection Impact // Doklady Earth Sciences, 2009b, Vol. 429, No. 8, pp. 1389–1393

Bondur V.G., Keeler R.N., Starchenkov S.A., Rybakova N.I. Monitoring of the Pollution of the Ocean Coastal Water Areas Using Space Multispectral High Resolution Imagery // Issledovanie Zemli is Cosmosa, 2006a, No 6, pp. 42-49 (In Russian).

Bondur V.G., Starchenkov S. Monitoring of Anthropogenic Influence on Water Areas of Hawaiian Islands Using RADARSAT and ENVISAT Radar Imagery. Proceed. of 31st Int. Symp. on Remote Sensing of Environment, St.Petersburg, 2006

Bondur V.G., Starchenkov S.A. Methods and software for aerospace imagery processing and classification. // Izvestia vuzov. Geodesy and Aerophotoimaging, 2001, No 3, pp. 118-143 (In Russian).

Bondur V.G., Tsidilina M. Features of Formation of Remote Sensing and Sea truth Databases for The Monitoring of Anthropogenic Impact on Ecosystems of Coastal Water Areas. Proceed. of 31st Int. Symp. on Remote Sensing of Environment, St.Petersburg, 2006

Bondur V.G., Zhurbas V.M., Grebenyuk Yu.V. Mathematical Modeling of Turbulent Jets of Deep-Water Sewage Discharge into Coastal Basins. ISSN 0001-4370, Oceanology, 2006b, Vol. 46, No. 6, pp. 757–771.

Bondur V.G., Zhurbas V.M., Grebenuk Yu.V. Modeling and Experimental Research of Turbulent Jet Propagation in the Stratified Environment of Coastal Water Areas // Oceanology, 2009a, Vol. 49, No. 5, pp. 595–606.

Bondur V.G., Zubkov E.V. Detection of small-scale inhomogeneities of optical characteristics of ocean upper layer by high resolution multispectral satellite imagery. Part I. Effects of drainage runoffs into coastal water areas// Issledovanie Zemli iz Cosmosa, 2005, No 4, pp. 54-61 (In Russian).

Bondur V.G., Zubkov E.V. Lidar methods of the ocean's upper layer pollution remote sensing // Optica atmospheri i oceana, 2001. Vol. 14, No 2, pp. 142-155 (In Russian)

Erlov N.G. Marine optics. Leningrad: Gidrometeoizdat, 1980. 249 p.

Fisher H., List E., Koh R., Imberger J., . Mixing in Inland and Coastal Waters. Academic Press, 1979. 484 p.

Gibson C.H., Bondur V.G., Keeler R.N., Leung P.T. Energetics of the Beamed Zombie Turbulence Maser Action Mechanism for Remote Detection of Submerged Oceanic Turbulence. Journal of Applied Fluid Mechanics, Vol. 1, No. 1, pp. 11-42, 2006.

Haltrin V.I. and Kattawar G.W. Self-consistent solutions to the equation of transfer with elastic and inelastic scattering in oceanic optics: I. Model // Applied Optics, 1993. Vol. 32. No. 27. P. 5356-5367.

Izrael Yu.A., Tsyban A.V. Anthropogenic ocean ecology. L: Gidrometeoizdat, 1989; 528 p.

Keeler R., Bondur V., and Gibson C., "Optical Satellite Imagery Detection of Internal Wave Effects from a Submerged Turbulent Outfall in the Stratified Ocean," Geophys. Res. Lett. 32, L12610, doi: 10.1029/2005GL022390 (2005).

Keeler R., Bondur V., Vithanage D. Sea truth measurements for remote sensing of littoral water //Sea technology, April 2004, p. 53-58.

Kopelevich O.V. Small-parameter Model of Optical Properties of sea water. Chapter 8 // Ocean Optics. V.1: Physical Ocean Optics / Ed. A.S.Monin. M.: Nauka Publishers. 1983.

Merrifield M.A., Alford M.H. Structure and variability of semidiurnal internal tides in Mamala Bay, Hawaii // J. Geophys. Res. 2004. V.109. C05010. doi:10.1029/2003JC002049

Ozmidov R.V. Diffusion of impurities in the ocean. M.: Gidrometeoizdat, 1986. 280 p.

Stern M. The "salt-fountain" and thermohaline convection // Tellus. 1960. ‹ 12. P. 172–175.

Vladimirov A.M, Ljahin J.I., Matveev L.T., Orlov V.G. Environmental control. L.:Hydrometeoizdad, 1991, p. 424.

Wolk F., Prandke H., Gibson C. Turbulence Measurements Support Satellite Observations // Sea Technology, v. 45, No 8, 2004

Zhurbas V.M. Trajectories of turbulent impurity jets in the stable stratified medium //Water resources. 1977. No 4. 165-172 pp.